THE JOURNAL OF PHYSICAL CHEMISTRY C
A JOURNAL OF THE AMERICAN CHEMICAL SOCIETY

pubs.acs.org/JPCC

Article

Isomerization and Redox Tuning: Reorganizing the Maya Blue Puzzle from Synthetic, Spectral, and Electrochemical Issues

Antonio Doménech-Carbó,* Ana María Costero, Salvador Gil, Noemí Montoya, Alejandro López-Carrasco, José A. Sáez, Pau Arroyo, and María Teresa Doménech-Carbó

Cite This: *J. Phys. Chem. C* 2021, 125, 26188−26200

Read Online

ACCESS | Metrics & More | Article Recommendations | Supporting Information

ABSTRACT: A new approach to describe the composition of Maya blue (MB), an ancient organic−inorganic hybrid material, is presented. It is based on the analysis of attenuated total reflection-Fourier transform infrared (ATR-FTIR), Raman spectroscopy, UV−visible (vis) spectroscopic, and electrochemical data for indigo and dehydroindigo plus palygorskite hybrids, including a novel methodology using electrocatalytic effects on the oxygen reduction reaction. As a result, it is concluded that MB results from the tautomerization of indigo-to-indigo hemienol and the subsequent oxidation of these isomeric forms to dehydroindigo, all associated with the palygorskite clay framework, at temperatures above 100 °C. This model is also consistent with ^{13}C NMR data on indigo plus sepiolite hybrids. A consistent set of thermochemical parameters is obtained from ATR-FTIR, solid-state electrochemistry, and UV−vis diffuse reflectance spectra for the successive isomerization and redox tuning processes experienced by palygorskite-associated indigo.

Downloaded via UNIV POLITECNICA VALENCIA on January 18, 2022 at 08:51:16 (UTC).
See https://pubs.acs.org/sharingguidelines for options on how to legitimately share published articles.

1. INTRODUCTION

Maya blue (MB), an ancient pigment used by the Mayas and other ancient Mesoamerican people in pre-Columbian times, can be considered as the precursor of a wide series of inorganic−organic hybrid materials.[1] Its remarkable stability, brightness, and hue variability have promoted a continuous interest in the pigment, which is surrounded by an atmosphere of mystery due to the absence of historical sources describing the preparation of the pigment by the Mayan people.[2,3]

The pigment results from the association of indigo (IND, 3*H*-indol-3-one-2-(1,3-dihydro-3-oxo-2*H*-indol-2-ylidene)-1,2-dihydro), a blue dye extracted from leaves of añil or xiuquitlitl (*Indigofera suffruticosa*) to palygorskite, a layered clay of ideal composition $Si_8(Mg_2Al_2)O_{20}(OH)_2(H_2O)_4{\cdot}4H_2O$. Pristine palygorskite contains three types of water molecules: physisorbed water on the surface of clay crystals, weakly bound water molecules in the channels (zeolitic water); and tightly bound water coordinated to the Mg^{2+} and Al^{3+} cations (structural water). From the preparative point of view, there is general agreement in which the preparation implies heating indigo (ca. 1 wt %) plus palygorskite mixtures up to 100 °C to promote the (more or less extensive) loss of water weakly bound to the clay channels. Usually, indigo@palygorskite hybrids are prepared by this "dry" method but the Mayans possibly used "wet" routes.[4,5]

Since the recognition of the organic−inorganic hybrid nature of the pigment,[6] the composition, structure, and optical properties of MB have become controversial with regard to the location of the indigo molecules on the palygorskite host and the type of dye−clay interaction.[7−14] These approaches were formulated within a general view, the "all-indigo" model, in which only one dye, indigo, was present in MB. In 2006, based on solid-state electrochemistry and spectroscopy data, we proposed an alternative view where a fraction of indigo was oxidized to dehydroindigo (DHI) so that the dehydroindigo/indigo ratio, in turn depending on the temperature of the thermal treatment used during the preparation of the pigment, is decisive to determine its hue.[15] The "dehydroindigo model", although reinforced in subsequent reports,[16−19] has not been unanimously accepted, alternating favorable[20−27] and neutral or opposite views.[28−36]

Testing these alternative models must face a series of important difficulties: (i) The organic components of the MB are associated with the clay support so that their properties—spectral in particular—are modified with respect to the isolated components so that the type of bonding and the location of the organic molecules in the palygorskite remain controversial;[7−9,13,14,27,29−35] (ii) dehydroindigo is a reactive compound whose synthesis is difficult; and[24,35] (iii) modeling of the attachment modes of the organic components to the clay via density functional theory (DFT) calculations is extremely sensitive to the hypotheses adopted to describe the dye-clay interactions (hydrogen bonding to structural water, binding to

Received: September 8, 2021
Revised: November 4, 2021
Published: November 18, 2021

ACS Publications

© 2021 American Chemical Society

silanol units, direct binding to Mg^{2+} and/or Al^{3+} cations, etc.).[13,20,22,27]

Studies on MB replicants are also extended to other indigo@clay hybrids, including sepiolite,[14,18,19,26,35] montmorillonite,[17−19,35] kaolinite,[35,37] and laponite,[35] the presence of dehydroindigo in several cases being confirmed by Raman spectroscopy[35] and liquid chromatography.[37,38] In the previous work,[39] we reported an updated revision of the available literature data, including UV−visible (vis), infrared, and Raman spectroscopies, nuclear magnetic resonance on sepiolite−indigo replicants, and solid-state electrochemistry. Our conclusion was that all experimental data can be interpreted in terms of the dehydroindigo model. However, Raman data challenged this scenario as far as the spectra of MB show an intriguing mixture of signatures attributable to indigo and dehydroindigo.[39]

In the current report, we present a modification of the dehydroindigo model based on additional synthetic, spectral, and electrochemical data. Such data depict a picture where the formation of MB proceeds via successive indigo (IND) tautomerization yielding indigo hemienol (HEIND) and oxidation to dehydroindigo (DHI), all associated with the palygorskite framework. This scenario is comparable to those described for the association of methyl red[40] and lapachol[41] with aluminosilicate clays where isomerization and redox tuning occur.

The synthesis of dehydroindigo and different indigo plus palygorskite and sepiolite MB-type specimens is accompanied by voltammetric data in the solution phase in the water−dimethyl sulfoxide (DMSO) mixtures and solid-state electrochemistry in contact with air-saturated aqueous acetate buffer at pH 4.75. Here, electrocatalytic effects on the oxygen reduction reaction (ORR) act as amplifiers of the differences between the different organic components. Visible and infrared spectra of MB replicants at temperatures between 100 and 180 °C are analyzed on the basis of this model and time-dependent DFT (TD-DFT) calculations resulting in consistent thermochemical data for the isomerization of redox tuning processes.

2. EXPERIMENTAL SECTION

2.1. Materials and Methods. Dehydroindigo was prepared as described in the literature.[42] Indigo (500 mg), PbO_2 (2.5 g), and $CaCl_2$ (500 mg) were suspended in toluene (50 mL). The reaction was heated under reflux for 10 min. Then, 250 mg of glacial acetic acid diluted in toluene was added and the mixture was heated for five additional minutes. The reaction was filtered under vacuum, and the solution volume was reduced to 15 mL. Dehydroindigo was isolated from the cold solution by filtration and washed several times with toluene (38.2% yield).

For preparing MB-type specimens, an indigo reagent (Aldrich), palygorskite (collected from the Yucatán site of Ticul), and sepiolite from Yunclillos (Spain) were used. Different IND@CLAY$_t$ specimens were prepared by crushing and mixing in agate mortar aliquots of ca. 1.0 g of the clay plus different amounts of indigo between 1 and 10 wt % during 1 h. The powdered mixture after the reaction was then subjected to heating in a furnace at temperatures between 100 and 200 °C for 24 h. Optionally, aliquots ca. 0.2 mg of the specimens were successively rinsed with DMSO and acetone to remove the dye remaining "externally" attached to the clay. Aliquots of IND@PAL$_{25}$ (1 wt % indigo) specimens were subjected to parallel heating under an argon atmosphere in an oven in contact with air at 150 °C for 24 h. The prepared materials are labeled IND@PAL$_{150}$(Ox) and IND@PAL$_{150}$(Ar), respectively.

Diffuse reflectance spectra were obtained with a PerkinElmer Lambda 35 spectrometer, a slit width of 1 nm, and a scan speed of 480 nm min^{-1}, in the case of solutions using 1 cm quartz cells. Attenuated total reflection-Fourier transform infrared (ATR-FTIR) spectra were collected with a Thermo Nicolet 6700 spectrophotometer with a deuterated triglycine sulfate (DTGS) detector with a detection range between 4000 and 400 cm^{-1}, equipped with a diamond window (16 accumulation scans). To acquire solid-state ^{13}C NMR spectra, approx. 200 mg of indigo, dehydroindigo, and IND@SEP$_{180}$ specimens were packed into a rotor container for solid NMR, and the corresponding spectra were acquired for 24 h in a Bruker Avance III WB 400 equipment.

Voltammetric experiments in the solution phase were carried out in ca. 1 mM solutions of indigo and dehydroindigo using a 0.10 M Bu_4NPF_6 (Fluka) solution in DMSO (Panreac) as the electrolyte. Here, a Pt-disk was used as a pseudoreference electrode, the potentials being normalized relative to the ferrocenium/ferrocene couple as the internal standard using 0.2 mM ferrocene solutions in the same electrolyte.

Electrocatalytic studies were carried out using glassy carbon electrodes (GCEs, BAS MF2012, a geometrical area of 0.071 cm^2) covered by a fine microparticulate deposit of IND@PAL$_t$ replicants. These were prepared by evaporation in air of 50 μL of a suspension (1 mg mL^{-1}) of the corresponding IND@PAL$_t$ specimen in ethanol. The IND@PAL$_t$-modified GCEs were immersed in air-saturated 0.25 M HAc/NaAc aqueous acetate buffer (Panreac reagents) in a pH 4.75 electrolyte and their voltammetric response was recorded.

Complementary voltammetric experiments were performed at 298 K in a three-electrode cell using a CHI 660C device (Cambria Scientific, Llwynhendy, Llanelli, U.K.). Air-saturated aqueous 0.25 M sodium acetate buffers (Panreac) at pH values between 4.0 and 6.0 were used as supporting electrolytes. Square wave voltammograms (SWVs) were recorded on sample-modified graphite electrodes (Maxim HB type leads, diameter 2 mm). The three-electrode arrangement was completed with a platinum wire auxiliary electrode and a Ag/AgCl (3 M NaCl) reference electrode. For electrode modification, an amount of 1−2 mg of the solid was extended on an agate mortar forming a fine spot of the solid material. Then, the lower end of the graphite electrode was gently rubbed over that spot of the sample and finally rinsed with water to remove ill-adhered particles. Sample-modified graphite bars were then dipped into the electrochemical cell so that only the lower end of the electrode was in contact with the electrolyte solution.

2.2. Computational Calculations. To gain insight into the UV−vis spectroscopic behavior of DHI, IND, and HEIND in solution, their structures were fully optimized at the RB3LYP/6-311++G(2df,2p) level in vacuo,[43,44] without symmetry restrictions using Gaussian 09, rev. D.01.[45] Frequency calculations from the optimized structures were performed to ensure that no imaginary frequencies were present. It must be taken into account that HEIND, a most stable structure (0.33 kcal mol^{-1} more stable than the completely planar one), has a dihedral angle of 27.6° between the two ring systems. The atomic coordinates of all species are detailed below. Over the optimized geometries of these structures, single-point TD-DFT calculations (30 states, singlets only)[46] at the same theory level in chloroform solution

https://doi.org/10.1021/acs.jpcc.1c07932
J. Phys. Chem. C 2021, 125, 26188−26200

using the polarizable continuum model (PCM) solvation model[47] within its nonequilibrium formalism were performed, which were used to generate UV−vis plots using the excitation energy and the oscillator strength for each excited state.

3. RESULTS AND DISCUSSION

3.1. Indigo−Palygorskite Hybrids. To test the dehydroindigo model, we compared the spectral properties of indigo (1 wt %) plus palygorskite specimens heated at different temperatures (in the following, IND@PAL$_t$) under an air and an Ar atmosphere. Our data are summarized in Figure 1, where the visible spectra of representative specimens are shown. The material heated in air showed the greenish hue and spectral features of MB, characterized by a main absorption band at 650 nm, unambiguously assigned to indigo,[10,11,20,21] and a lower band at ca. 475 nm coincident with the absorption spectra of dehydroindigo.[15−18,24] Remarkably, the specimens prepared under an Ar atmosphere exhibited a slightly less intense greenish tint and similar spectral features. Here, the intensity of the band at 650 nm increased while the second band decreased, and its maximum was slightly shifted to 500 nm relative to the specimens prepared in Ar.

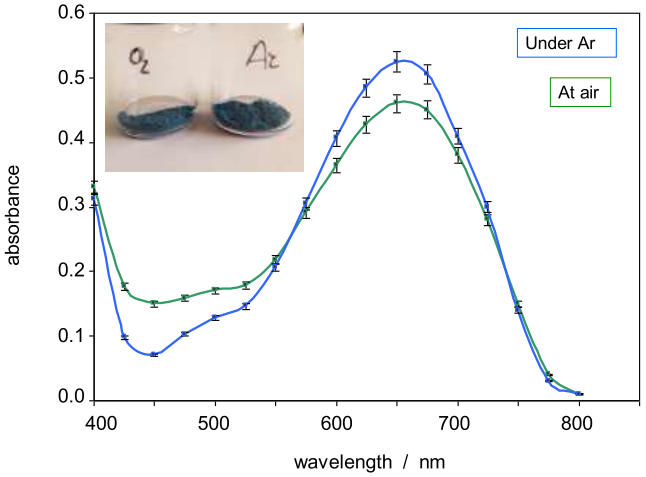

Figure 1. Visible spectra of the two aliquots of indigo (1 wt %) plus the palygorskite mixture heated at 130 °C for 3 h in a closed reactor under an Ar and air atmosphere in an open furnace. Inset: photographic image of the heated specimens. Error bars correspond to three replicate absorbance measurements at wavelength intervals of 25 nm.

Additional experiments were performed in specimens containing indigo loadings of 5 and 10 wt %. The maximum proportion of indigo entirely occupying the palygorskite channels is of ca. 4.5 wt %[27,48,49] so that these specimens necessarily contain a significant proportion of "external" indigo. In fact, rinsing with organic solvents or concentrated HNO_3 suggests that only ca. 1 wt % indigo is "internally" retained in MB specimens.[13,31−34] However, in contrast with indigo, which retains its blue color, heating such indigo plus palygorskite specimens above 100 °C leads these materials to acquire a more or less intense greenish tint.

The next step was the preparation of dehydroindigo plus palygorskite (in the following, DHI@PAL$_t$) replicants. Unfortunately, dehydroindigo is an elusive compound whose synthesis leads to a purple solid, which slowly degrades to indigo, as well as its solutions in organic solvents, in agreement with the reported data.[24,35] Surprisingly, the attachment of dehydroindigo (1 wt %) to palygorskite initially yields a pale purple solid that turns blue in a few minutes, as illustrated in Figure S1, Supporting Information. This process can be attributed to the reaction with water physisorbed on the clay as well as, to some extent, with water molecules in the clay channels, as evidenced by the variation in the visible spectra of dehydroindigo solutions in DMSO in the presence of water

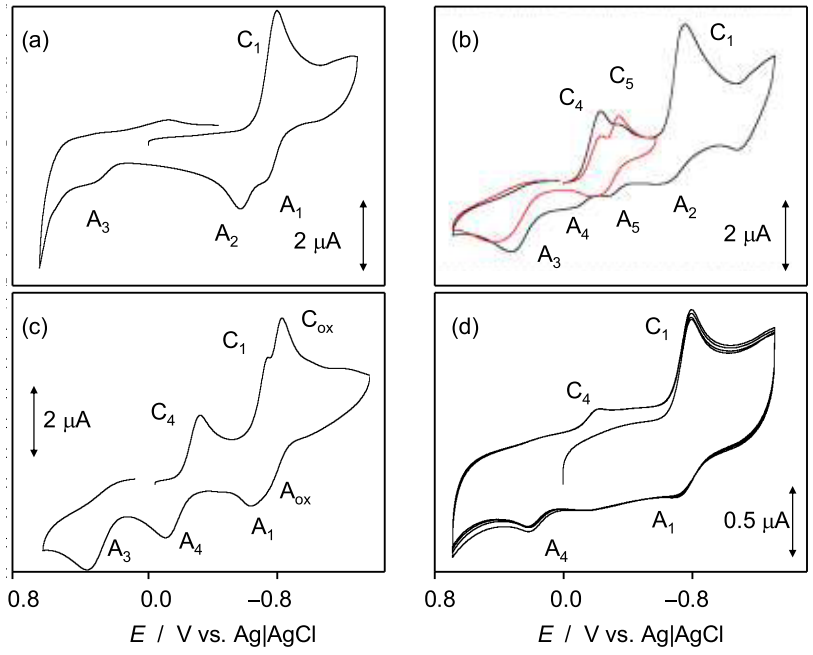

Figure 2. Cyclic voltammograms at GCE in 0.10 M Bu_4NPF_6/DMSO containing 1% v/v of water solutions. (a) 0.5 mM indigo; (b) freshly prepared 0.5 mM dehydroindigo; (c) same solution after 5 min under an Ar atmosphere; and (d) DMSO extract from an IND@PAL$_{150}$ specimen.

https://doi.org/10.1021/acs.jpcc.1c07932
J. Phys. Chem. C 2021, 125, 26188−26200

(see Figure S2, Supporting Information), equivalent to literature data.[24]

The fact that the greenish MB-type specimens can be prepared under an Ar atmosphere and the high sensitivity of dehydroindigo to water traces suggested that another component contributed to the greenish hue of the MB.

3.2. Solution-Phase Electrochemistry. Cyclic voltammetric data in water-containing DMSO solutions of indigo and dehydroindigo revealed a complex scenario. As can be seen in Figure 2a, the cyclic voltammograms at GCE of 0.10 M Bu_4NPF_6/DMSO containing 1% v/v of water solution displays a cathodic peak at −0.77 V (C_1) followed, in the subsequent anodic scan, by overlapping peaks at −0.68 V (A_1) and −0.57 V (A_2) preceding an anodic signal at 0.35 V (A_3) with no coupled cathodic counterpart C_3. This voltammetry contrasts with that widely studied under anhydrous conditions, limited to the one-electron reversible couple C_1/A_1.[50] In turn, dehydroindigo solutions in water-containing DMSO (Figure 2b) show two overlapped cathodic peaks at −0.22 (C_4) and −0.34 V (C_5) coupled to anodic waves at −0.20 (A_4) and −0.08 V (A_5), accompanied by the oxidation peak A_3. This last signal also appears in the initial anodic scan voltammograms and, if the potential scan is prolonged to sufficiently negative values, the C_1/A_1 couple is recorded but decreases upon lowering the water content of the parent solution. Upon aging, the couple C_1/A_1 exhibits both cathodic and anodic peak splitting (Figure 2c). Interestingly, the DMSO extracts of IND@PAL_t and DHI@PAL specimens show the C_1/A_1 and C_4/A_4 couples (see Figure 2d).

This voltammetry can be interpreted using the scheme depicted in Figure 3. In the presence of water, the one-electron

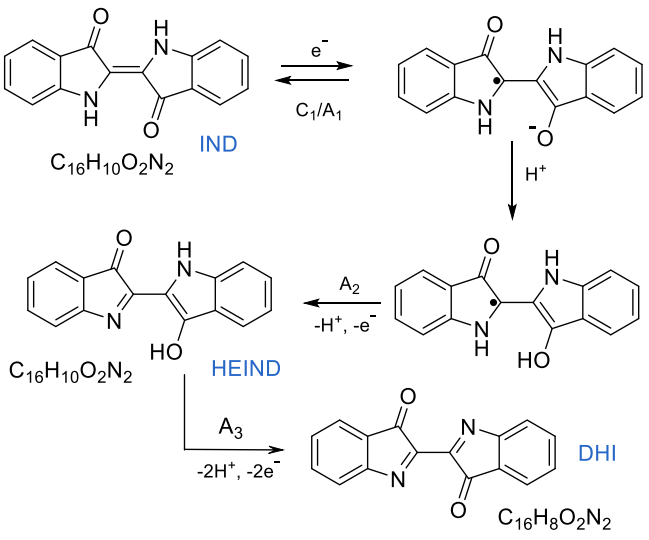

Figure 3. Scheme to describe the indigo- (upper part) and dehydroindigo-localized (lower part) electrochemical processes in Figure 2.

reversible reduction of indigo to its radical anion (C_1/A_1 couple) is accompanied by the protonation of this second species that is oxidized to an indigo tautomer, termed provisionally as indigo hemienol, which in turn is irreversibly oxidized to dehydroindigo via the process A_3. Dehydroindigo solutions will contain a more or less large fraction of indigo so that the indigo-localized electrochemical pathway is superimposed to that of dehydroindigo, consisting of the reversible reduction to the corresponding radical anion (process C_4/A_4). This is also protonated then yielding indigo hemienol giving rise to a new couple C_5/A_5 and the oxidation process A_3 regenerating dehydroindigo. The appearance of new signals C_{ox}/A_{ox} close to the C_1/A_1 couple increasing with time can be attributed to the formation of O_2, whose one-electron reduction in aprotic solvents occurs at these potentials,[51] and the corresponding process being $2DHI + H_2O \rightarrow 2IND + O_2$.

These voltammetric data introduce a new component into the MB puzzle, indigo hemienol. Although formally equivalent to a keto−enol tautomerization, the formation of indigo hemienol from indigo involves a drastic structural change because the breaking of the central C=C converts the plane indigo molecule into another much more flexible one, just the demand for an efficient entrance into the palygorskite channels.[52] This matter will be treated in relation to Raman spectra (vide infra).

3.3. Indigo Hemienol. The above data suggest that the initial step in the formation of MB is the formation of indigo hemienol. Table 1 summarizes the literature data on the visible

Table 1. Literature Data of the UV−Vis Spectra of the Different Studied Systems

system	λ_{max} (nm)	λ_{max} (nm)	λ_{max} (nm)	source
indigo in toluene solution	600			Rondão et al.[24]
indigo in MeOH solution	607			Rondão et al.[24]
indigo in DMF solution	611	444^{sh}		Miliani et al.[36]
indigo in $CHCl_3$ solution	603	426^{sh}		Miliani et al.[36]
indigo solid	657	560^{sh}		De Faria et al.[35]
IND@PAL_{130}	667		435	Reinen et al.[10]
	667		500	De Faria et al.[35]
	661		490	Miliani et al.[36]
dehydroindigo in toluene			455	Rondão et al.[24]
dehydroindigo in MeOH			400	Rondão et al.[24]
dehydroindigo in $CHCl_3$			450	De Faria et al.[35]
dehydroindigo solid			475	De Faria et al.[35]
			558	Rondão et al.[24]

spectra of indigo and dehydroindigo in solution, while Figure 4a depicts the simulated UV−vis spectra of indigo, dehydroindigo, and indigo hemienol in $CHCl_3$ solution from TD-DFT calculations (see the Supporting Information). The absorbance maxima of indigo and dehydroindigo under CHC_{l3} solvation are located at 600 and 500, respectively, in reasonable agreement with experimental data (see Table 1).[35,36] The maximum absorbance calculated for indigo hemienol appears at 660 nm, similar to that observed in the spectra of MB-type specimens (see Figure 1). Consistently, the extracts resulting from rinsing with $CHCl_3$ of MB-type specimens display visible spectra in close agreement with the theoretical spectrum of HEIND in this solvent. Figure 4b compares the spectra of the $CHCl_3$ extracts of blue IND@PAL_{25} and greenish IND@PAL_{150} (both 1 wt % indigo) specimens normalized to equal the absorbance maxima. The spectrum of the extract from the nonheated IND@PAL_{25} specimen is identical to the theoretical spectrum of indigo, with a unique absorbance maximum at 600 nm. The spectrum of the extract from the

https://doi.org/10.1021/acs.jpcc.1c07932
J. Phys. Chem. C 2021, 125, 26188−26200

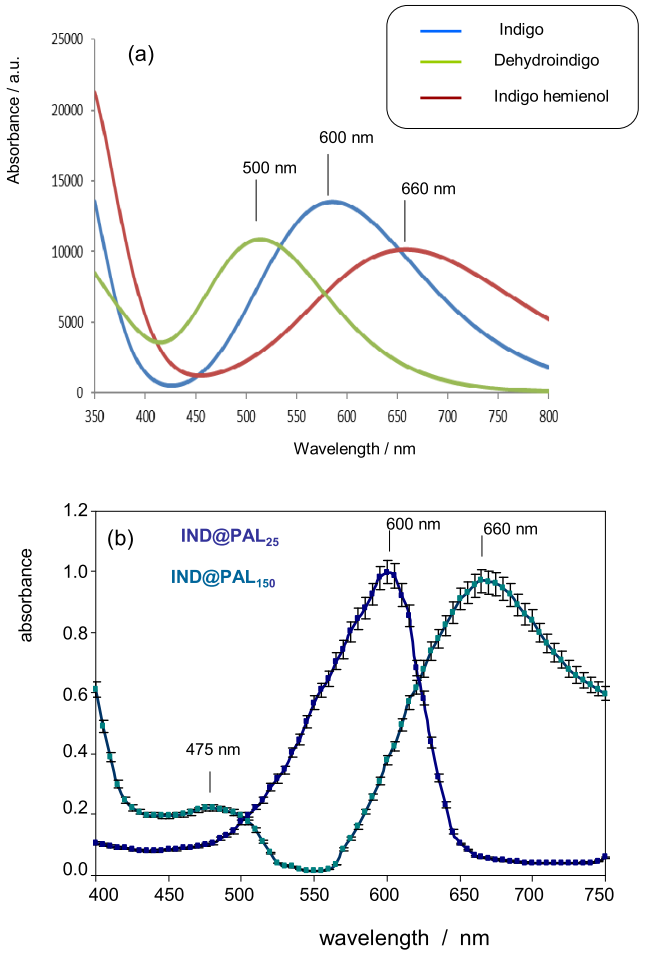

Figure 4. (a) Simulated UV−vis spectra of indigo, dehydroindigo, and indigo hemienol in $CHCl_3$ solution. (b) Spectrum of the $CHCl_3$ extracts of IND@PAL_{25} and IND@PAL_{150} specimens. Error bars in panel (b) correspond to three replicate absorbance measurements at wavelength intervals of 25 nm.

IND@PAL_{150} replicant is essentially coincident with the solid-state spectra (Figure 1) and exhibits an absorbance maximum at 660 nm. This is accompanied by a secondary maximum at ca. 475 nm. This feature is in agreement with the expected presence of a certain proportion of dehydroindigo accompanying indigo hemienol.

Additionally, the HEIND hypothesis is supported by the spectral data recently reported by De Faria et al.[35] and Miliani et al.[36] for synthetic IND@PAL_t specimens revealing that the intensity of the absorption band at ca. 500 nm increases relative to that of the band at ca. 650 nm on increasing the temperature of preparation of the hybrid materials (vide infra).

Comparing the Raman spectra of indigo in solution with those of dehydroindigo and MB-type synthetic specimens and archeological MB samples[11−14,28,35,53] resulted in a puzzling situation. Although the relative intensity of the bands was dependent on the wavelength of the radiation excitation, common features were obtained in literature data. In MB specimens prepared at temperatures below 180 °C,[14,35] and genuine MB specimens,[11−14,28,36,53] there are bands at 1680, 1630, 1595, 1575, 1490, 1461, 1378, 1360, and 1250 cm^{-1}. Up to 180 °C, additional bands at 1700 and 1420 cm^{-1} are recorded.[35] Several bands are close to those appearing in the spectrum of indigo in solution, namely, at 1698, 1627, 1578, 1448, 1362, 1310, and 1248 cm^{-1},[35] and several are common with those recorded for solid dehydroindigo, appearing at 1732, 1597, 1530, 1448, and 1378 cm^{-1}.[35]

Figure 5 compares the schematized Raman spectra of (a) indigo in solution, (b) solid dehydroindigo, and (c) IND@PAL_{180} specimens showing the aforementioned features. At the expense of a detailed analysis of the Raman spectrum of HEIND, one can expect that this spectrum contains bands quite similar to both indigo and dehydroindigo.

The analysis of vibrational spectroscopy data is complicated by the similarity of the spectral features of the different indigoid compounds, as underlined by Tomkinson et al.[54] According to the theoretical study reported by these authors, the more representative bands to discern the presence of dehydroindigo in MB are the γ(NH) mode appearing in the 450−550 cm^{-1} region and the degenerate composite of the *u* and *g* components of a γ(C−H) mode of the benzene motif at ca. 750 cm^{-1}.[54] These bands are weak or absent in the Raman spectra of several genuine MB specimens,[14,28] in agreement with the dehydroindigo and the current models.

It is more difficult to use the data from ATR-FTIR spectra due to the superposition of palygorskite bands (see Figure S3, Supporting Information). The first band is obscured by the absorption of palygorskite but the second can be clearly recorded in ATR-FTIR spectra of IND@PAL specimens. In Figure 6, we compare the 800−730 cm^{-1} region of the ATR-FTIR spectra of (a) dehydroindigo, (b) indigo, and (c) IND@PAL_{25} (5 wt % indigo) and IND@PAL_{160} (5 wt % indigo). Both indigo and unheated blue IND@PAL_{25} specimens display a well-defined band at 767 cm^{-1}, which is absent in the spectrum of dehydroindigo. This band, which can be ascribed to the aforementioned γ(C−H) mode, appears as diminished—without entire disappearance—in the spectra of greenish IND@PAL_t specimens and displays peak splitting on increasing the temperature. Taking into account that the IND@PAL_{160} specimen contains an excess of "external" indigo, the low intensity of the 767 cm^{-1} band can be considered as consistent with the proposed model of progressive formation of indigo hemienol and dehydroindigo upon increasing the temperature of preparation of the specimen.

The spectral features of MB were initially interpreted as due to the deformation of the indigo molecules as a result of the interaction with the palygorskite.[11−14,52] However, theoretical calculations revealed that the observed spectral changes cannot solely be produced by a loss of planarity of the indigo molecule.[14] In the dehydroindigo view, the MB spectrum results from the superposition of the spectra of indigo and dehydroindigo molecules in different proportions and is more or less distorted as a result of the anchorage of these molecules to the clay framework.[15−18] Current data support the idea that the formation of MB via heating a mixture of indigo and palygorskite proceeds via tautomerization to indigo hemienol and subsequent oxidation to dehydroindigo, all attached to the clay framework.

The HEIND hypothesis is also supported by ^{13}C NMR spectroscopy on MB-type specimens prepared from sepiolite, a channeled silicate with tunnel dimensions larger than those of palygorskite routinely used in MB studies[7,18,19,26,30,32,34,35,38] because NMR spectra are not accessible to palygorskite specimens. Figure 7 shows the ^{13}C NMR spectra of the (a) IND@SEP_{180} (10 wt % indigo) specimen and (b) indigo. The most remarkable features fall in the region of the carbonyl carbon (ca. 190 ppm). In this region, indigo shows an isolated

https://doi.org/10.1021/acs.jpcc.1c07932
J. Phys. Chem. C 2021, 125, 26188−26200

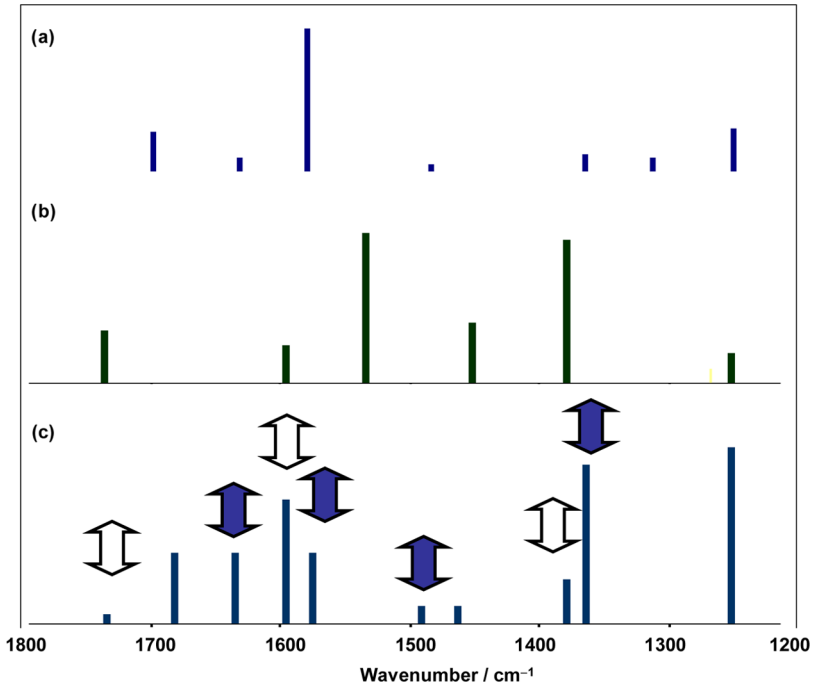

Figure 5. Schematics of Raman spectra of (a) indigo in solution, (b) solid dehydroindigo, and (c) IND@PAL$_{180}$ specimen schematized from data in ref 35. Solid arrows mark the Raman peaks coincident with indigo and white arrows those coincident with dehydroindigo.

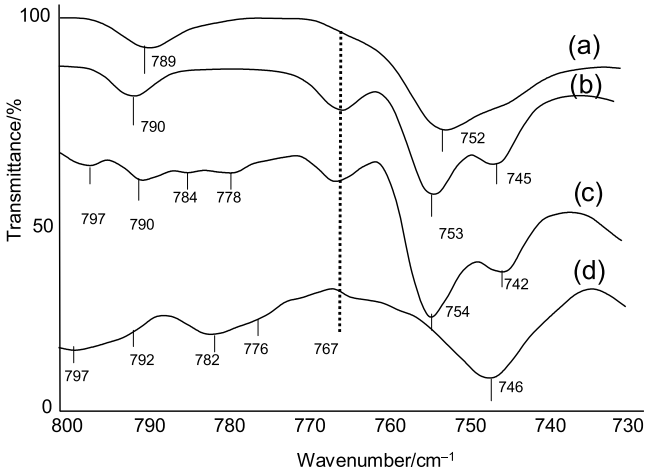

Figure 6. ATR-FTIR spectra of (a) dehydroindigo, (b) indigo, (c) IND@PAL$_{25}$ (5 wt % indigo), and (d) IND@PAL$_{160}$ (5 wt % indigo). The transmittance axis is displayed for clarity.

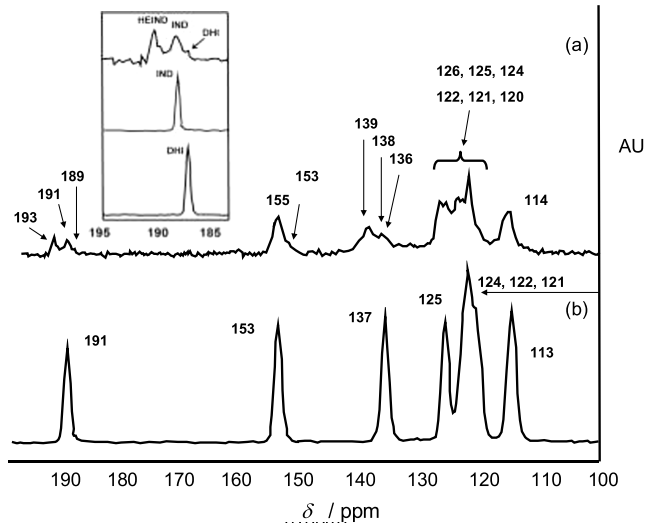

Figure 7. Solid-state ^{13}C NMR spectra of (a) IND@PAL$_{180}$ (10 wt % indigo) replicant and (b) indigo. Inset: details of the C-carbonyl region of (from top to bottom) IND@PAL$_{180}$ (10 wt % indigo), indigo, and dehydroindigo.

peak at 191 ppm while dehydroindigo shows an equally isolated peak at 189 ppm (see the inset in Figure 7). In turn, the IND@SEP$_{180}$ replicant displays overlapping peaks at 193, 191, and 189 ppm. The peak at 193 ppm can be attributed to indigo hemienol. All of these spectra agree with those reported for indigo[7] and dehydroindigo[24] and indigo plus sepiolite specimens reported by Hubbard et al.,[7] Hirschinger et al.,[55] and Giustetto et al.[40] (see Table S1, Supporting Information). These features confirm the presence of these components in MB-type specimens prepared from sepiolite, which mimics those prepared from palygorskite.

3.4. Electrocatalytic Effects. Solid-state electrochemistry offers additional data consistent with the indigo hemienol hypothesis. As expected from previous studies,[15−19] microparticulate deposits of indigo, dehydroindigo, and their unheated "blue" IND@PAL$_{25}$ and DHI@PAL$_{25}$ specimens attached to graphite electrodes in contact with aqueous acetate buffer at pH values between 4 and 6 display essentially identical responses. These consist of pH-dependent peaks at ca. 0.40 and −0.35 V corresponding to the proton-assisted oxidation of indigo to dehydroindigo and the reduction of indigo to leucoindigo (see Figure S4, Supporting Information).[15−19] These signals show some peak splitting in the voltammograms of the heated DHI@PAL$_t$ and IND@PAL$_t$ specimens, a feature that is particularly intense in the specimens at high indigo loadings and increases with the temperature of preparation of the specimens, as can be seen in Figures S5 and S6 of the Supporting Information. This feature can be interpreted in terms of the coexistence in such

https://doi.org/10.1021/acs.jpcc.1c07932
J. Phys. Chem. C 2021, 125, 26188−26200

specimens of significant amounts of both indigo and indigo hemienol, whose oxidation and reduction signals will appear at slightly different potentials (vide infra).

To amplify the differences between the different palygorskite-associated indigoid species, we analyzed the electrocatalytic effects exerted on the reduction of dissolved oxygen (oxygen reduction reaction, ORR). This constitutes a novel approach in MB chemistry aimed to discriminate between different organic components based on their different electrocatalytic performances on a given redox probe. In Figure 8, we

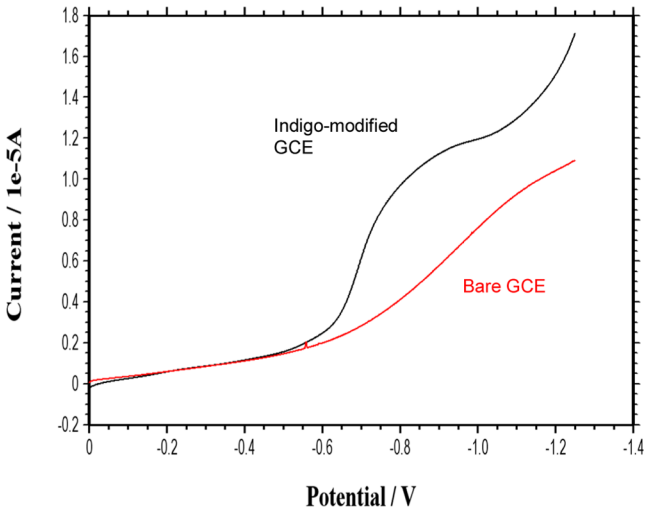

Figure 8. Linear potential scan voltammograms at bare GCE and indigo-modified GCE in contact with a 0.25 M HAc/NaAc aqueous buffer at pH 4.75. Potential scan initiated at 0.0 V in the negative direction; potential scan rate is 50 mV s^{-1}.

compare the linear potential scan voltammograms, recorded at the bare GCE and at an indigo-modified GCE in contact with the air-saturated 0.25 M HAc/NaAc aqueous buffer at pH 4.75. One can see that the cathodic wave recorded at ca. −1.0 V at the bare GCE, corresponding to the ORR, is positively shifted and moderate although it significantly increased at the indigo-modified electrode. These features, which also appear for all indigo@palygorskite specimens, can be interpreted in terms of the existence of an electrocatalytic effect on the ORR process due to the organic component.

In Figure 9, we compare the corresponding voltammograms, after semiderivative data convolution, recorded for microparticulate deposits of indigo, IND@PAL_{25}, IND@PAL_{180}(Ar), and IND@PAL_{180}(Ox) (all 1 wt % indigo) in an air-saturated aqueous acetate buffer at pH 4.75. In the case of indigo, a main cathodic peak appears at −0.72 V, preceded by cathodic waves at ca. −0.2 and −0.4 V. These waves are clearly enhanced in the case of the blue IND@PAL_{25} specimen, for which the main cathodic signal is shifted to −0.61 V and followed by a shoulder at −0.72 V. Remarkably, the response of the MB-type specimen heated under an Ar atmosphere (IND@PAL_{180}(Ar)) was essentially restricted to the cathodic peak at −0.66 V with clearly weaker signals at −0.2 and −0.4 V. This last feature is retained in the voltammogram of the specimen heated in air (IND@PAL_{180}(Ox)), but here the main cathodic signal is displaced to −0.74 V, being preceded by a shoulder at ca. −0.66 V.

These features can be interpreted taking into consideration that solid indigo is electrochemically reduced to leucoindigo through a two-proton, two-electron process at ca. −0.25 V. Although indigo is insoluble under our experimental conditions, leucoindigo possesses some low solubility, so that the peaks at −0.2 and −0.4 V can in principle be attributed to the competing reduction of solid indigo to solid and soluble forms of leucoindigo

$$\{C_{16}H_{10}O_2N_2\}_{solid} + 2H^+_{aq} + 2e^- = \{C_{16}H_{12}O_2N_2\}_{solid} + C_{16}H_{12}O_2N_{2\,aq} \quad (1)$$

In these circumstances, a possible catalytic pathway on the ORR process may involve the electrochemically generated leucoindigo, as schematized in Figure 10. The occurrence of this process is reflected in the voltammograms of indigo and IND@PAL_{25} (Figure 9a,b) by the enhancement of the indigo-centered cathodic signals at −0.2 and −0.4 V. The large intensity of the main cathodic signal at around −0.7 V and the clear depletion of the signals at −0.2 and −0.4 V in the case of the MB-type specimens, IND@PAL_{180}(Ar) and IND@PAL_{180}(Ox) (Figure 9c,d), suggest that a second catalytic pathway operates.

This can be rationalized by considering the multistep nature of the ORR process. This is initiated by the one-electron reduction of O_2 to the superoxide radical anion, being followed by competing protonation, disproportionation, and subsequent electron transfer processes successively yielding not only H_2O_2 and H_2O but also reactive species such as hydroperoxide ($HO_2^{\bullet}$) and hydroxyl ($HO^{\bullet}$) radicals and hydroperoxide anions (HO_2^-). One plausible electrocatalytic way is similar to that described by Compton et al.[56] for the catalysis of hematite on the ORR at GCE in neutral media. Here, hematite acts as a chemical catalyst accelerating the disproportionation of H_2O_2 into H_2O and O_2.

Following a similar scheme, the different indigo forms can simultaneously act as electron mediators via electrochemical reduction of indigo to leucoindigo, or as chemical catalysts favoring the disproportionation of intermediate $O_2^{\bullet-}$ (and/or $HO_2^{\bullet}$ and H_2O_2). This second pathway can be considered to be responsible for the enhancement and potential shift of the ORR peak ca. −0.7 V.

For our purposes, the relevant point to emphasize is that this second pathway discriminates between different indigoid species and that the observed features can be interpreted within the isomerization plus redox tuning scenario described here. First of all, both indigo and IND@PAL_{25}, where solid indigo microparticles are accessible to the electrode/electrolyte junction, display both types of catalytic actions. In the case of IND@PAL_{25}, however, the association with the palygorskite determines a positive shift of the ORR peak that moves from −0.72 V for indigo to −0.61 V for the blue IND@PAL_{25} specimen. This shift can be attributed to the fact that in this specimen a part of the indigo becomes separated into clay-associated individual molecules, thus breaking the hydrogen bonding system existing in solid indigo.

In the case of the heated greenish MB-type specimens, only the second catalytic pathway is relevant. In the case of the specimen heated in an Ar atmosphere, the ORR peak potential is −0.66 V, thus suggesting that the species responsible for this catalytic effect differs from individual indigo molecules associated with the clay. In our scheme, the dominating species will be the indigo hemienol. Consistently, the specimen heated at air displays overlapping ORR peaks at −0.66 and −0.75 V. The former corresponds to the indigo tautomer

https://doi.org/10.1021/acs.jpcc.1c07932
J. Phys. Chem. C 2021, 125, 26188−26200

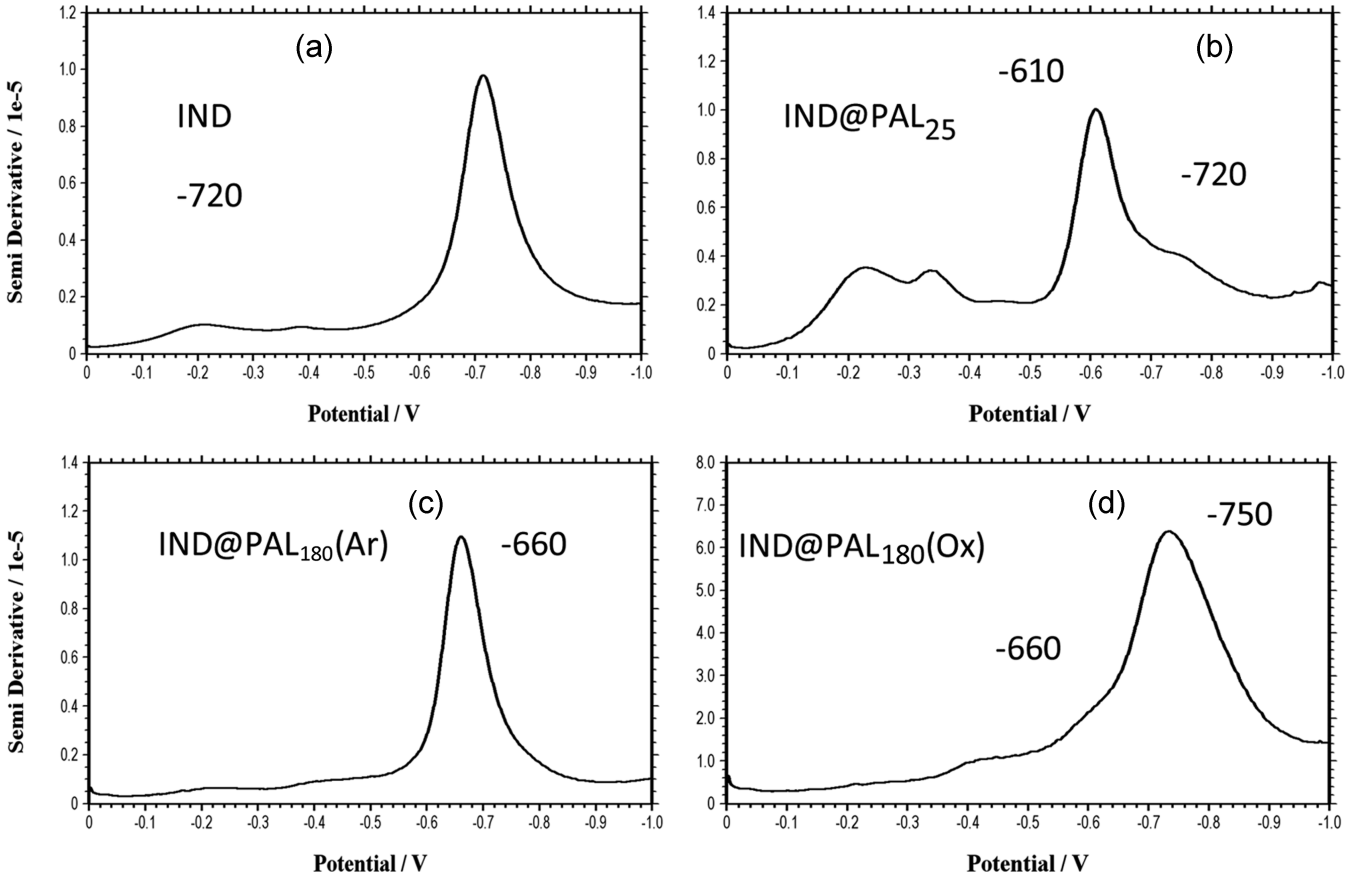

Figure 9. Linear potential scan voltammograms, after the semiderivative convolution, of microparticulate deposits of (a) indigo, (b) IND@PAL$_{25}$, (c) IND@PAL$_{180}$(Ar), and (d) IND@PAL$_{180}$(Ox) (all hybrid specimens containing 1 wt % indigo) on GCE in contact with a 0.25 M HAc/NaAc aqueous buffer at pH 4.75. Potential scan initiated at 0.0 V in the negative direction; potential scan rate is 50 mV s^{-1}.

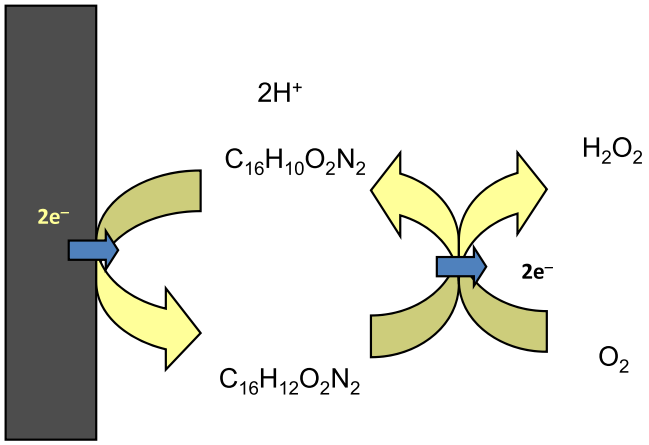

Figure 10. Scheme for one of the possible electrocatalytic pathways exerted by indigo on the ORR process.

whereas the second can be assigned to the catalytic effect exerted by palygorskite-attached dehydroindigo.

3.5. Thermochemical Parameters. The MB closure described here assumes that heating indigo plus the palygorskite mixtures successively yields indigo hemienol and dehydroindigo, the material thus acquiring the characteristic greenish color. This two-step process is entirely consistent with the reported electrochemical, UV−vis, and Raman spectral data.[35,36] The data in Figure 11a,b correspond to the ratio between the absorbance at 500 and 660 nm, A_{500}/A_{660}, of IND@PAL$_t$ specimens from our experiments and those reported by De Faria et al.[35] and Miliani et al.[36] Coincidentally, the A_{500}/A_{660} ratio increases with the temperature defining two steps. Assuming that at temperatures below 180 °C the generation of indigo hemienol predominates over that of dehydroindigo, the A_{500}/A_{660} absorbance ratio will be representative of the advance of tautomerization. At temperatures above 180 °C, the absorbance ratio will represent the advance of the oxidation to dehydroindigo. These processes can be represented as

$$\{\text{IND@PAL}\cdot y\text{H}_2\text{O}\}_{\text{solid}} \rightarrow \{\text{HEIND@PAL}\cdot z\text{H}_2\text{O}\}_{\text{solid}} + (y - z)\text{H}_2\text{O}_{\text{gas}} \quad (2)$$

$$\{\text{HEIND@PAL}\cdot z\text{H}_2\text{O}\}_{\text{solid}} + 1/2\text{O}_{2\text{gas}} \rightarrow \{\text{DHI@PAL}\cdot w\text{H}_2\text{O}\}_{\text{solid}} + (z - w)\text{H}_2\text{O}_{\text{gas}} \quad (3)$$

Thermochemical data can be calculated from spectral data assuming that both HEIND and DHI display a characteristic band between 450 and 540 nm and that the IND and HEIND main band is located at ca. 660 nm. In principle, the equilibrium constants for the reaction described by eq 2 can roughly be estimated from the absorbance ratios, A_{500}/A_{660}, provided that the factor relating the relative amount of each species with the absorbance is known. One can write

https://doi.org/10.1021/acs.jpcc.1c07932
J. Phys. Chem. C 2021, 125, 26188−26200

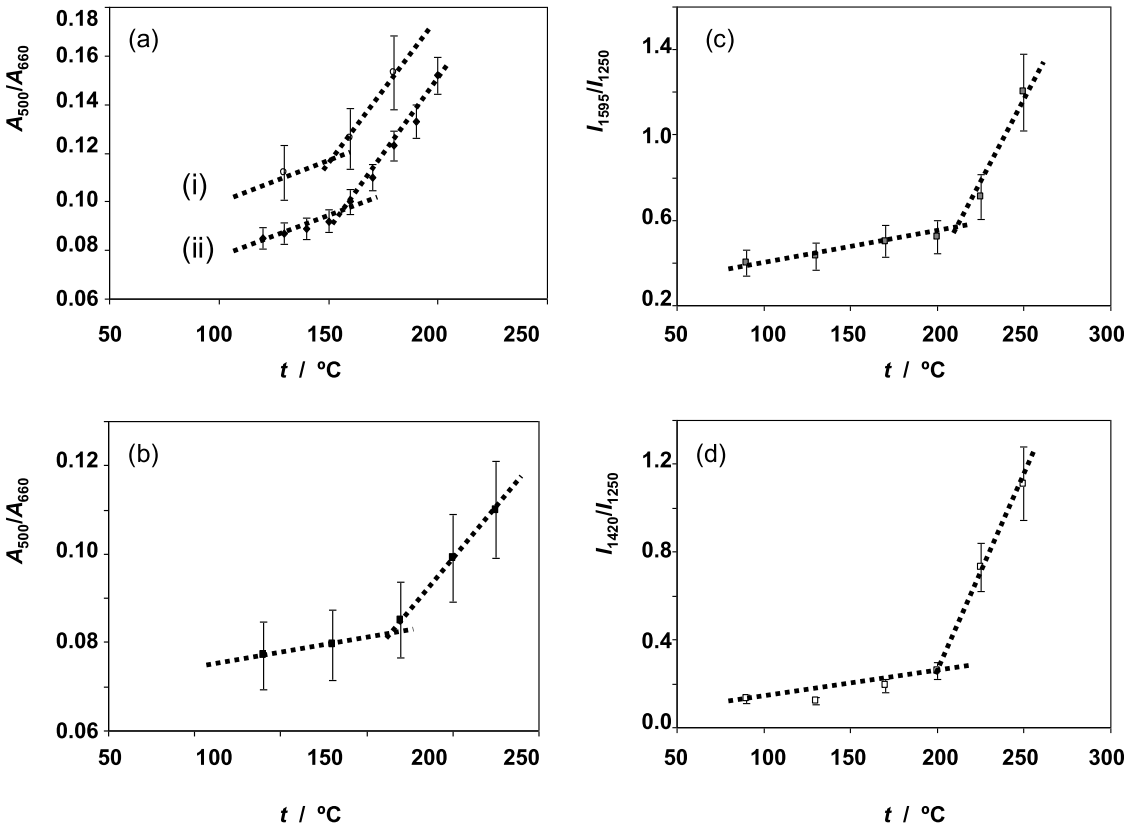

Figure 11. Variation of the A_{500}/A_{660} ratio in the visible spectra of IND@PAL$_t$ replicants from (a) Miliani et al.[36] (i), our data (ii), and (b) De Faria et al.,[35] and variation of the (c) I_{1595}/I_{1250} and (d) I_{1420}/I_{1250} ratios in the Raman spectra of IND@PAL$_t$ replicants from De Faria et al.[35] Error bars for our data correspond to dispersion from three replicate experiments. Error bars for literature data where uncertainty was not reported are depicted assuming relative uncertainties of 10%.

$$\frac{A_{500}}{A_{650}} = \frac{\varepsilon_{500}^{\mathrm{HEIND}} c_{\mathrm{HEIND}}}{\varepsilon_{660}^{\mathrm{HEID}} c_{\mathrm{HEIND}} + \varepsilon_{660}^{\mathrm{IND}} c_{\mathrm{IND}}} \tag{4}$$

where c represents the concentration of each absorbing species and ε its respective molar absorptivity coefficient. Assuming that $\varepsilon = \varepsilon_{500}^{\mathrm{HEIND}}/\varepsilon_{660}^{\mathrm{IND}} \approx \varepsilon_{500}^{\mathrm{HEIND}}/\varepsilon_{660}^{\mathrm{HEIND}}$, one can estimate the molar fraction of HEIND as

$$\alpha_{\mathrm{HEIND}} = \varepsilon\left(\frac{A_{500}}{A_{660}}\right) \tag{5}$$

In principle, ε can be approximated from the values of the molar absorptivity reported in the literature for indigo and dehydroindigo in solution, so that $\varepsilon = 0.25 \pm 0.10$. Then, assuming that the system behaves such as a closed homogeneous system reaching the equilibrium at all temperatures, the apparent equilibrium constant for the isomerization reaction can be calculated at each temperature as

$$K_{\mathrm{TAU}} = \frac{\alpha_{\mathrm{HEIND}}}{1 - \alpha_{\mathrm{HEND}}} = \frac{\frac{1}{\varepsilon}\left(\frac{A_{500}}{A_{660}}\right)}{1 - \frac{1}{\varepsilon}\left(\frac{A_{500}}{A_{660}}\right)} \tag{6}$$

Then, one can calculate the values of K_{TAU} and hence the corresponding approximate (apparent) values of $\Delta G^{\circ}_{\mathrm{TAU}}$ (as $\Delta G^{\circ}_{\mathrm{TAU}} = -RT \ln K_{\mathrm{TAU}}$) at different temperatures. The data in Figure 11a,b can be used to determine the K_{TAU} and $\Delta G^{\circ}_{\mathrm{TAU}}$ values. The representation of $\Delta G^{\circ}_{\mathrm{TAU}}$ vs T can be fitted to two straight lines (see Figure S6 in the Supporting Information) whose slope and ordinate at the origin yield, respectively, the $\Delta^{\circ}{}_{\mathrm{TAU}}$ and $\Delta^{\circ}{}_{\mathrm{TAU}}$ of the respective processes, assumed to be essentially temperature independent ($\Delta G^{\circ} = \Delta H^{\circ} - T\Delta S^{\circ}$). Similar considerations can be applied to determine the corresponding parameters, K_{OX1}, $\Delta G^{\circ}_{\mathrm{OX1}}$, for the oxidation process described by eq 3. Table 2 summarizes the thermochemical parameters determined from the different sets of UV−vis data in Figure 11a,b.

Similar considerations can be applied to the ratio between the intensities of the Raman bands at 1595 and 1250 cm^{-1}, I_{1595}/I_{1250}, represented in Figure 11c, assuming that the former is common to indigo hemienol and dehydroindigo and the

Table 2. Thermochemical Parameters Calculated from Visible and Raman Spectroscopies and Voltammetric Data for the Processes of Tautomerization and the Subsequent Oxidation to Dehydroindigo Oxidation in MB

	$\Delta G^{\circ}_{\mathrm{TAU}}$ (kJ mol^{-1})	$\Delta G^{\circ}_{\mathrm{OX1}}$ (kJ mol^{-1})	$\Delta G^{\circ}_{\mathrm{OX2}}$ (kJ mol^{-1})
A_{500}/A_{660}[a]	3.0 ± 0.6	9.8 ± 0.8	12.8 ± 1.2
A_{500}/A_{660}[b]	2.9 ± 0.6	6.2 ± 0.6	9.1 ± 1.0
A_{500}/A_{660}[c]	5.7 ± 1.6	10 ± 2	16 ± 3
I_{1595}/I_{1250}[d]	3.5 ± 0.8	14 ± 6	18 ± 6
I_{1420}/I_{1250}[d]			14.6 ± 1.4
$E^{\circ}_{\mathrm{II}} - E^{\circ}_{\mathrm{I}}$[eF]	5.0 ± 1.0		

[a]From visible spectra in this study. [b]From visible spectra in ref 35. [c]From visible spectra in ref 36. [d]From Raman spectra in ref 35. [eF]rom voltammetric data in this study.

https://doi.org/10.1021/acs.jpcc.1c07932
J. Phys. Chem. C 2021, 125, 26188−26200

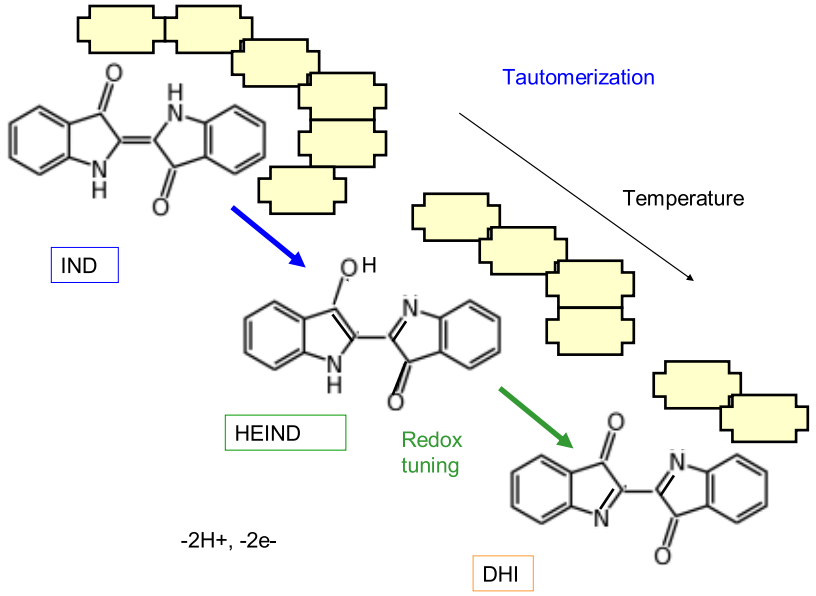

Figure 12. Schematic representation of the formation of MB via tautomerization and redox tuning of indigo associated with the palygorskite clay.

second is representative of indigo. In turn, the band at 1420 cm^{-1} can be attributed to dehydroindigo so that the I_{1420}/I_{1250} ratio (see Figure 11d) will represent the advance of the redox tuning. In this scheme, the equilibrium constants of the reactions described by eqs 2 and 3 can be estimated from the I_{1595}/A_{1250} values provided that the factor relating the relative amount of each species with the Raman intensity, ε, is known. Then

$$\frac{I_{1595}}{I_{1250}} = \frac{\varepsilon_{1595}^{HEIND} c_{HEIND} + \varepsilon_{1595}^{DHI} c_{DHI}}{\varepsilon_{1250}^{IND} c_{IND}} \quad (7)$$

At temperatures below 180 °C, we can assume that indigo hemienol largely prevails over dehydroindigo so that

$$\frac{I_{1595}}{I_{1250}} \approx \frac{\varepsilon_{1595}^{HEIND} c_{HEIND}}{\varepsilon_{1250}^{IND} c_{IND}} \quad (8)$$

Assuming that the ε coefficients are equal, the equilibrium constant for the isomerization reaction will be

$$K_{TAU} \approx \frac{I_{1595}}{I_{1250}} \quad (9)$$

As before, the apparent values of ΔG°_{TAU} calculated as $\Delta G^{\circ}_{TAU} = -RT \ln K_{TAU}$ from data in ref 35 at different temperatures define two straight lines (see Figure S7, Supporting Information) allowing the estimation of the thermochemical parameters in Table 2. Remarkably, these values agree with those estimated from UV−vis data. The sum of the ΔG°_{TAU} and ΔG°_{OX1} values formally corresponds to the direct conversion of indigo into dehydroindigo attached to the clay matrix. The Gibbs energy of this process, ΔG°_{OX2}, can be calculated from the above data or directly computing the ratio between the Raman intensities at 1420 and 1250 cm^{-1}, I_{1420}/I_{1250}, because the band at 1420 cm^{-1} can be attributed to dehydroindigo. As can be seen in Table 1, despite the necessary application of rough approximations, the ΔG°_{TAU}, ΔG°_{OX1}, and ΔG°_{OX2} values calculated from different techniques agree reasonably.

In fact, this agreement can be extended to the ΔG°_{TAU} value that can be calculated from solid-state electrochemistry data. For this purpose, we can consider the solid-state oxidation process of IND@PAL$_t$ and DHI@PAL$_t$ hybrids in contact with aqueous acetate buffer (see Figures S4 and S5). For unheated IND@PAL$_{25}$ specimens, the equilibrium potential corresponds to the electrochemical reduction process

$$DHI@PAL_{solid} + 2H^{+}_{aq} + 2e^{-} \rightarrow IND@PAL_{solid} \quad (10)$$

so that $\Delta G^{\circ}_{I} = -nFE^{\circ}_{I}$, where E°_{I} represents the equilibrium potential of the electrochemical process. For specimens prepared by heating above 100 °C, one can assume that indigo has converted into indigo hemienol. Then, the electrochemical process will be

$$DHI@PAL_{solid} + 2H^{+}_{aq} + 2e^{-} \rightarrow HEIND@PAL_{solid} \quad (11)$$

Now, $\Delta G^{\circ}_{II} = -nFE^{\circ}_{II}$, where E°_{I} represents the equilibrium potential of the electrochemical process described by eq 11. Accordingly, the Gibbs free energy change associated with the tautomerization process described by eq 2 can be expressed as

$$\Delta G^{\circ}_{TAU} = \Delta G^{\circ}_{II} - \Delta G^{\circ}_{I} = nF(E^{\circ}_{II} - \Delta E^{\circ}_{I}) \quad (12)$$

As already described in detail,[15−19] these processes behave reversibly, so that the peak potentials can be taken as representative of the equilibrium potentials. Our averaged experimental values from experiments such as in Figure S4 and the peak potential values recorded for genuine MB archeological specimens[15] are $E^{\circ}_{II} - \Delta E^{\circ}_{I} = 25 \pm 5$ mV. Then, $\Delta G^{\circ}_{TAU} = 5.0 \pm 1.0$ kJ mol^{-1}, a value in agreement with those calculated from UV−vis and Raman spectral data (see Table 2).

3.6. Discussion. The above data are consistent with a description of MB in terms of successive isomerization and redox tuning processes as schematized in Figure 12. Generically, this view is consistent with the description of isomerization of methyl red plus palygorskite hybrids reported by Giustetto et al.,[40] and the isomerization and redox tuning previously studied for lapachol attached to palygorskite,[39] and

https://doi.org/10.1021/acs.jpcc.1c07932
J. Phys. Chem. C 2021, 125, 26188−26200

are also consistent with the two-step kinetics observed from spectral data in the preparation of MB specimens.[57] This model is also consistent with thermochemical data that can be estimated from electrochemical, Raman, and visible spectroscopic data.

The proposed model is able to explain another controversial aspect of MB. The origin of the greenish color was attributed to the red shift of the main absorbance band of indigo from ca. 600 to 660 nm with the concomitant displacement of the reflectance maximum from ca. 450 to 550 nm.[10] In the all-indigo model, this spectral feature results from the interaction of the indigo molecule with the palygorskite clay. In our model, this spectral feature is the result of the formation of HEIND (accompanied by DHI) whose spectrum in solution (compare Figures 1 and 4b) is essentially identical to those of MB.

When the central C═C bond of indigo is replaced with a single C−C one, the indigo hemienol molecule acquires sufficient flexibility to penetrate into the palygorskite channels but retains the capability of reorganization in this limited space prompting its subsequent oxidation to dehydroindigo. As previously discussed on comparing literature data for different IND@CLAY$_t$ specimens,[39] the size of the indigo molecules (4.8 Å) relative to the channel's width determines their color. As reported by Martinetto et al.,[58] mordenite, having 7.0 × 6.5 Å^2 channels, does not form stable hybrids because the channels are so wide that they retain indigo molecules. Consistently, LTA zeolite (channels of 4.1 × 4.1 Å^2) cannot form hybrids with indigo because the organic molecules cannot enter into the clay channels. Sepiolite (10.6 × 3.7 Å^2), palygorskite (6.4 × 3.7 Å^2), and silicalite (5.3 × 5.6 Å^2), however, form stable hybrids resistant to HNO_3 attack.[58] Remarkably, the indigo plus silicalite hybrids retain the blue color after heating above 100 °C. This is in contrast with the palygorskite and sepiolite hybrids that upon heating acquire the greenish tint characteristic of MB-type replicants. This can be interpreted within the scenario proposed here on assuming that the tautomerization of indigo (and the subsequent oxidation to dehydroindigo) require a certain space as suggested by calculations on indigo and dehydroindigo entrapment into palygorskite channels.[27] In the case of silicalite, the channels are not large enough to facilitate the tautomerization and only blue specimens are obtained.[58] In the case of palygorskite and sepiolite, the size of the channels permits to carry out the isomerization and oxidation processes resulting in the formation of greenish specimens.

Accordingly, the previously advocated[15−19,38,39] view of the MB as a polyfunctional hybrid material where different organic components are attached to the inorganic matrix has to be corrected, and extended:extensive tautomerization of indigo to indigo hemienol accompanied by redox tuning to dehydroindigo determines the peculiar properties (optical in particular) of the pigment. Although this view decreases the importance of dehydroindigo in MB, it substantially differs from the all indigo view where only the indigo molecule more or less deformed is assumed to associate with the palygorskite framework.

4. CONCLUSIONS

A novel approximation to the nature of MB where, upon heating indigo plus palygorskite mixtures above 100 °C, indigo isomerizes to indigo hemienol, which in turn is oxidized to clay-associated dehydroindigo at higher temperatures is presented. This view is based on UV−vis diffuse reflectance spectra, ATR-FTIR, and solid-state electrochemistry of MB-type specimens in contact with aqueous acetate buffer, as well as on the solution phase and solid-state electrochemistry of indigo and dehydroindigo. In this view, the formation of both indigo hemienol and dehydroindigo results in the appearance of the greenish tint characteristic of MB-type specimens. This description of MB is also consistent with ^{13}C NMR data for MB replicants prepared from indigo and sepiolite. The electrocatalytic effect exerted by the MB-type materials on the reduction of dissolved oxygen permits the discrimination between the different organic components introducing a novel approach in the study of hybrid materials.

Thermochemical analysis of such data permits us to estimate the Gibbs free energy for the reactions of tautomerization and redox tuning of palygorskite-associated hybrid materials. This view reinforces the description of the MB as a polyfunctional hybrid material where different organic components are attached to the inorganic matrix and emphasizes the role of tautomerization and redox tuning processes in the chemistry of hybrid materials. Apart from its relevance with respect to the MB problem, the current approach illustrates the variety and flexibility of the chemistry involved in organic−inorganic hybrid materials.

■ ASSOCIATED CONTENT

Supporting Information

The Supporting Information is available free of charge at https://pubs.acs.org/doi/10.1021/acs.jpcc.1c07932.

Computational calculations; UV−vis spectra of dehydroindigo in DMSO solution; ATR-FTIR spectra of indigo and selected MB-type specimens; ΔG_{TAU} vs T plots from UV−vis and Raman spectroscopy data; and table of ^{13}C data (PDF)

■ AUTHOR INFORMATION

Corresponding Author

Antonio Doménech-Carbó − *Departament de Química Analítica, Universitat de València, 46100 Burjassot, València, Spain;* orcid.org/0000-0002-5284-2811; Email: antonio.domenech@uv.es

Authors

Ana María Costero − *Instituto Interuniversitario de Investigación de Reconocimiento Molecular y Desarrollo Tecnológico, 46100 Burjassot, València, Spain;* orcid.org/0000-0001-9640-1148

Salvador Gil − *Instituto Interuniversitario de Investigación de Reconocimiento Molecular y Desarrollo Tecnológico, 46100 Burjassot, València, Spain*

Noemí Montoya − *Facultad de Ciencias de la salud, Universidad Internacional de la Rioja (UNIR), 26006 Logroño, La Rioja, Spain*

Alejandro López-Carrasco − *Instituto Interuniversitario de Investigación de Reconocimiento Molecular y Desarrollo Tecnológico, 46100 Burjassot, València, Spain*

José A. Sáez − *Instituto Interuniversitario de Investigación de Reconocimiento Molecular y Desarrollo Tecnológico, 46100 Burjassot, València, Spain*

Pau Arroyo − *Instituto Interuniversitario de Investigación de Reconocimiento Molecular y Desarrollo Tecnológico, 46100 Burjassot, València, Spain*

https://doi.org/10.1021/acs.jpcc.1c07932
J. Phys. Chem. C 2021, 125, 26188−26200

María Teresa Doménech-Carbó − *Institut de Restauració del Patrimoni, Universitat Politècnica de València, 46022 València, Spain*

Complete contact information is available at: https://pubs.acs.org/10.1021/acs.jpcc.1c07932

Notes

The authors declare no competing financial interest.

■ ACKNOWLEDGMENTS

Projects PID2020-113022GB-I00 and RTI2018-100910-B-C42, supported by MCIN/AEI/10.13039/501100011033 are gratefully acknowledged for all of the equipment employed. NMR was registered at the U26 facility of ICTS "NANBIOSIS" at the SCSIE of the Universitat of València.

■ REFERENCES

(1) Gómez-Romero, P.; Sánchez, C. Hybrid materials. Functional properties. From Maya Blue to 21st century materials. *New J. Chem.* **2005**, *29*, 57−58.

(2) Reyes-Valerio, C. *De Bonampak al Templo Mayor: el azul Maya en Mesoamérica*; Siglo XXI Editores: Mexico, 1993.

(3) Arnold, D. E.; Branden, J. R.; Williams, P. R.; Feinman, G. M.; Brown, J. P. The first direct evidence for the production of Maya Blue: rediscovery of a technology. *Antiquity* **2008**, *82*, 151−164.

(4) Doménech-Carbó, A.; Doménech-Carbó, M. T.; Vidal-Lorenzo, C.; Vázquez De Agredos-Pascual, M. L.; Osete-Cortina, L.; Valle-Algarra, F. M. Discovery of indigoid-containing clay pellets from La Blanca: significance with regard to the preparation and use of Maya Blue. *J. Archaeol. Sci.* **2014**, *41*, 147−155.

(5) Doménech-Carbó, A.; Doménech-Carbó, M. T.; Vázquez de Agredos-Pascual, M. L. From Maya Blue to 'Maya Yellow': A Connection between Ancient Nanostructured Materials from the Voltammetry of Microparticles. *Angew. Chem., Int. Ed.* **2011**, *50*, 5741−5744.

(6) Shepard, A. O. Maya Blue: alternative hypotheses. *Am. Antiq.* **1962**, *27*, 565−566.

(7) Hubbard, B.; Kuang, W.; Moser, A.; Facey, G. A.; Detellier, C. Structural study of Maya Blue: textural, thermal and solidstate multinuclear magnetic resonance characterization of the palygorskite-indigo and sepiolite-indigo adducts. *Clays Clay Miner.* **2003**, *51*, 318−326.

(8) Chiari, G.; Giustetto, R.; Ricchiardi, G. Crystal structure refinement of palygorskite and Maya Blue from molecular modelling and powder synchrotron diffraction. *Eur. J. Mineral.* **2003**, *15*, 21−33.

(9) Fois, E.; Gamba, A.; Tilocca, A. On the unusual stability of Maya blue paint: molecular dynamics simulations. *Microporous Mesoporous Mater.* **2003**, *57*, 263−272.

(10) Reinen, D.; Köhl, P.; Müller, C. The Nature of the Colour Centres in 'Maya Blue' the Incorporation of Organic Pigment Molecules into the Palygorskite Lattice. *Z. Anorg. Allg. Chem.* **2004**, *630*, 97−103.

(11) Leona, M.; Casadio, F.; Bacci, M.; Picollo, M. Identification of the Pre-Columbian Pigment Maya Blue on Works of Art by Noninvasive UV-Vis and Raman Spectroscopic Techniques. *J. Am. Inst. Conserv.* **2004**, *43*, 39−54.

(12) Vandenabeele, P.; Bode, S.; Alonso, A.; Moens, L. Raman spectroscopic analysis of the Maya wall paintings in Ek'Balam, Mexico. *Spectrochim. Acta, Part A* **2005**, *61*, 2349−2356.

(13) Giustetto, R.; Llabres i Xamena, F. X.; Ricchiardi, G.; Bordiga, S.; Damin, A.; Gobetto, R.; Chierotti, M. R. Maya Blue: A Computational and Spectroscopic Study. *J. Phys. Chem. B* **2005**, *109*, 19360−19368.

(14) Sánchez del Río, M.; Picquart, M.; Haro-Poniatowski, E.; van Eslande, E.; Uc, V. H. On the Raman spectrum of Maya blue. *J. Raman Spectrosc.* **2006**, *37*, 1046−1053.

(15) Doménech-Carbó, A.; Doménech-Carbó, M. T.; Vázquez De Agredos-Pascual, M. L. Dehydroindigo: a New Piece into the Maya Blue Puzzle from the Voltammetry of Microparticles Approach. *J. Phys. Chem. B* **2006**, *110*, 6027−6039.

(16) Doménech-Carbó, A.; Doménech-Carbó, M. T.; Vázquez De Agredos-Pascual, M. L. Chemometric Study of Maya Blue from the Voltammetry of Microparticles Approach. *Anal. Chem.* **2007**, *79*, 2812−2821.

(17) Doménech-Carbó, A.; Doménech-Carbó, M. T.; Vázquez De Agredos-Pascual, M. L. Indigo/Dehydroindigo/Palygorskite Complex in Maya Blue: An Electrochemical Approach. *J. Phys. Chem. C* **2007**, *111*, 4585−4595.

(18) Doménech-Carbó, A.; Doménech-Carbó, M. T.; Sanchez del Rio, M.; Goberna, S.; Lima, E. Evidence of Topological Indigo/Dehydroindigo Isomers in Maya Blue-Like Complexes Prepared from Palygorskite and Sepiolite. *J. Phys. Chem. C* **2009**, *113*, 12118−12131.

(19) Doménech-Carbó, A.; Doménech-Carbó, M. T.; Sanchez del Rio, M.; Vázquez De Agredos-Pascual, M. L. Comparative study of different indigo-clay Maya Blue-like systems using the voltammetry of microparticles approach. *J. Solid State Electrochem.* **2009**, *13*, 869−878.

(20) Tilocca, A.; Fois, E. The Color and Stability of Maya Blue: TDDFT Calculations. *J. Phys.Chem. C* **2009**, *113*, 8683−8687.

(21) Polette-Niewold, L. A.; Manciu, F. S.; Torres, B.; Alvarado, M., Jr.; Chianelli, R. R. Organic/inorganic complex pigments: Ancient colors Maya Blue. *J. Inorg. Biochem.* **2007**, *101*, 1958−1973.

(22) Fuentes, M. E.; Peña, B.; Contreras, C.; Montero, A. L.; Chianelli, R.; Alvarado, M.; Olivas, R.; Rodríguez, L. M.; Camacho, H.; Montero-Cabrera, L. A. Quantum mechanical model for Maya Blue. *Int. J. Quantum Chem.* **2008**, *108*, 1664−1673.

(23) Manciu, F. S.; Reza, L.; Polette, L. A.; Torres, B.; Chianelli, R. R. Raman and infrared studies of synthetic Maya pigments as a function of heating time and dye concentration. *J. Raman Spectrosc.* **2007**, *38*, 1193−1198.

(24) Rondão, R.; de Melo, J. S. S.; Bonifacio, V. D. B.; Melo, M. J. Dehydroindigo, the Forgotten Indigo and Its Contribution to the Color of Maya Blue. *J. Phys. Chem. A* **2010**, *114*, 1699−1708.

(25) Giustetto, R.; Wahyudi, O. Sorption of red dyes on palygorskite: Synthesis and stability of red/purple Mayan nano-composites. *Microporous Mesoporous Mater.* **2011**, *142*, 221−235.

(26) Giustetto, R.; Wahyudi, O.; Corazzari, I.; Turci, F. Chemical stability and dehydration behavior of a sepiolite/indigo Maya Blue pigment. *Appl. Clay Sci.* **2011**, *52*, 41−50.

(27) Sánchez-Ochoa, F.; Cocoletzi, G. H.; Canto, G. Trapping and diffusion of organic dyes inside of palygorskite clay: The ancient Maya Blue pigment. *Microporous Mesoporous Mater.* **2017**, *249*, 111−117.

(28) Wiedemann, H. G.; Brzezinka, K. -W.; Witke, K.; Lamprecht, I. Thermal and Raman-spectroscopic analysis of Maya Blue carrying artefacts, especially fragment IV of the Codex Huamantla. *Thermochim. Acta* **2007**, *456*, 56−63.

(29) Sánchez del Río, M.; Boccaleri, E.; Milanesio, M.; Croce, G.; van Beek, W.; Tsiantos, C.; Chyssikos, G.; Gionis, V.; Kacandes, G.; Suárez, M.; García-Romero, E. A combined synchrotron powder diffraction and vibrational study of the thermal treatment of palygorskite−indigo to produce Maya blue. *J. Mater. Sci.* **2009**, *44*, 5524−5536.

(30) Ovarlez, S.; Giulieri, F.; Chaze, A.−M.; Delamare, F.; Raya, J.; Hirschinger, J. The Incorporation of Indigo Molecules in Sepiolite Tunnels. *Chem.—Eur. J.* **2009**, *15*, 11326−11332.

(31) Dejoie, C.; Martinetto, P.; Dooryhée, E.; Strobel, P.; Blanca, S.; Bordat, P.; Brown, R.; Porcher, F.; Sanchez del Rio, M.; Anne, M. Indigo@Silicalite: a New Organic-Inorganic Hybrid Pigment. *ACS Appl. Mater. Interfaces* **2010**, *2*, 2308−2316.

(32) Ovarlez, S.; Giulieri, F.; Delamare, F.; Sbirrazzuoli, N.; Chaze, A.-M. Indigo−sepiolite nanohybrids: Temperature-dependent synthesis of two complexes and comparison with indigo−palygorskite systems. *Microporous Mesoporous Mater.* **2011**, *142*, 371−380.

(33) Tsiantos, C.; Tsampodimou, M.; Kacandes, G. H.; Sánchez del Río, M.; Gionis, V.; Chryssikos, G. D. Vibrational investigation of

indigo−palygorskite association(s) in synthetic Maya blue. *J. Mater. Sci.* **2012**, *47*, 3415−3428.
(34) Lima, E.; Guzmán, A.; Vera, M.; Rivera, J. L.; Fraissard, J. Aged Natural and Synthetic Maya Blue-Like Pigments: What Difference Does It Make? *J. Phys. Chem. C* **2012**, *116*, 4556−4563.
(35) Bernardino, N. D.; Constantino, V. R. L.; De Faria, D. L. A. Probing the Indigo Molecule in Maya Blue Simulants with Resonance Raman Spectroscopy. *J. Phys. Chem. C* **2018**, *122*, 11505−11515.
(36) Grazia, C.; Buti, D.; Amat, A.; Rosi, F.; Romani, A.; Domenici, D.; Sgamellotti, A.; Miliani, C. Shades of blue: non-invasive spectroscopic investigations of Maya blue pigments. From laboratory mock-ups to Mesoamerican codices. *Heritage Sci.* **2020**, *8*, No. 1.
(37) Doménech-Carbó, A.; Doménech-Carbó, M. T.; Valle-Algarra, F. M.; Domine, M. E.; Osete-Cortina, L. On the dehydroindigo contribution to Maya Blue. *J. Mater. Sci.* **2013**, *48*, 7171−7183.
(38) Doménech-Carbó, A.; Valle-Algarra, F. M.; Doménech-Carbó, M. T.; Domine, M. E.; Osete-Cortina, L.; Gimeno-Adelantado, J. V. Redox tuning and species distribution in Maya Blue-type materials: a reassessment. *ACS Appl. Mater. Interfaces* **2013**, *5*, 8134−8145.
(39) Doménech-Carbó, A.; Holmwood, S.; Di Turo, F.; Montoya, N.; Valle-Algarra, F. M.; Edwards, H. G. M.; Doménech-Carbó, M. T. Composition and Color of Maya Blue: Reexamination of Literature Data Based On the Dehydroindigo Model. *J. Phys. Chem. C* **2019**, *123*, 770−782.
(40) Giustetto, R.; Seenivasan, K.; Pellerej, D.; Ricchiardi, G.; Bordiga, S. Spectroscopic characterization and photo/thermal resistance of a hybrid palygorskite/methyl red Mayan pigment. *Microporous Mesoporous Mater.* **2012**, *155*, 167−176.
(41) Doménech-Carbó, A.; Valle-Algarra, F. M.; Doménech-Carbó, M. T.; Osete-Cortina, L.; Domine, M. E. 'Maya chemistry' of organic−inorganic hybrid materials: isomerization, cyclicization and redox tuning of organic dyes attached to porous silicates. *RSC Adv.* **2013**, *3*, 20099−20105.
(42) Kalb, L. Über dehydro-indigo, ein neues oxidation-sprodukt des indigos. *Ber. Dtsch. Chem. Ges.* **1909**, *42*, 3642.
(43) McLean, A. D.; Chandler, G. S. Contracted Gaussian-basis sets for molecular calculations. 1. 2nd row atoms, Z = 11-18. *J. Chem. Phys.* **1980**, *72*, 5639−5648.
(44) Blaudeau, J.-P.; McGrath, M. P.; Curtiss, L. A.; Radom, L. Extension of Gaussian-2 (G2) theory to molecules containing third-row atoms K and Ca. *J. Chem. Phys.* **1997**, *107*, 5016−5021.
(45) Frisch, M. J.; Trucks, G. W.; Schlegel, H. B.; Scuseria, G. E.; Robb, M. A.; Cheeseman, J. R.; Scalmani, G.; Barone, V.; Petersson, G. A.; Nakatsuji, H. et al. *Gaussian 09*, revision D.01; Gaussian, Inc.: Wallingford, CT, 2016.
(46) Laurent, A. D.; Adamo, C.; Jacquemin, D. Dye chemistry with time-dependent density functional theory. *Phys. Chem. Chem. Phys.* **2014**, *16*, 14334−14356.
(47) Scalmani, G.; Frisch, M. J. Continuous surface charge polarizable continuum models of solvation. I. General formalism. *J. Chem. Phys.* **2010**, *132*, No. 114110.
(48) Yasarawan, N.; Van Duijneveldt, J. S. Dichroism in Dye-Doped Colloidal Liquid Crystals. *Langmuir* **2008**, *24*, 7184−7192.
(49) Mondelli, C.; Sánchez del Río, M.; González, M. A.; Magazzú, A.; Cavallari, C.; Suárez, M.; García-Romero, E.; Romano, P. Role of water on formation and structural features of Maya blue. *J. Phys.: Conf. Ser.* **2012**, *340*, No. 012109.
(50) Bond, A. M.; Marken, F.; Hill, E.; Compton, R. G.; Hügel, H. The electrochemical reduction of indigo dissolved in organic solvents and as a solid mechanically attached to a basal plane pyrolytic graphite electrode immersed inaqueous electrolyte solution. *J. Chem. Soc., Perkin Trans. 2* **1997**, 1735−1742.
(51) Sawyer, D. T.; Chiericato, G.; Angelis, C. T.; Nanni, E. J.; Tsuchiya, T. Effects of Media and Electrode Materials on the Electrochemical Reduction of Dioxygen. *Anal. Chem.* **1982**, *54*, 1720−1724.
(52) Witke, K.; Brzezinka, K.-W.; Lamprecht, I. Is the indigo molecule perturbed in planarity by matrices? *J. Mol. Struct.* **2003**, *661−662*, 235−238.
(53) Garcia Moreno, R.; Strivay, D.; Gilbert, B. Maya blue-green pigments found in Calakmul, Mexico: a study by Raman and UV−visible spectroscopy. *J. Raman Spectrosc.* **2008**, *39*, 1050−1056.
(54) Tomkinson, J.; Bacci, M.; Picollo, M.; Colognesi, D. The vibrational spectroscopy of indigo: A reassessment. *Vib. Spectrosc.* **2009**, *50*, 268−276.
(55) Raya, J.; Hirschinger, J.; Ovarlez, S.; Giulieri, F.; Chaze, A.-M.; Delamare, F. Insertion of indigo molecules in the sepiolite structure as evidenced by 1H−29Si heteronuclear correlation spectroscopy. *Phys. Chem. Chem. Phys.* **2010**, *12*, 14508−14514.
(56) Shimizu, K.; Sepunaru, L.; Compton, R. G. Onnovative catalyst design for the oxygen reduction reaction for fuel cells. *Chem. Sci.* **2016**, *7*, 3364−3369.
(57) Doménech, A.; Doménech-Carbó, M. T.; Osete-Cortina, L.; Montoya, N. Application of solid-state electrochemistry techniques to polyfunctional organic−inorganic hybrid materials: The Maya Blue problem. *Microporous Mesoporous Mater.* **2013**, *166*, 123−130.
(58) Dejoie, C.; Dooryhée, E.; Martinetto, P.; Blanc, S.; Bordat, P.; Brown, R.; Porcher, F.; Sanchez del Rio, M.; Strobel, P.; Anne, M.; Van Eslande, E.; Walter, P. Revisiting Maya Blue and Designing Hybrid Pigments by Archaeomimetism. hal-00495128.v1, 2010, http://hal.archives-ouvertes.fr/.

https://doi.org/10.1021/acs.jpcc.1c07932
J. Phys. Chem. C 2021, 125, 26188−26200